nature materials

LETTERS

PUBLISHED ONLINE: 28 JUNE 2009 | DOI: 10.1038/NMAT2489

An omnidirectional retroreflector based on the transmutation of dielectric singularities

Yun Gui Ma[1], C. K. Ong[2], Tomáš Tyc[3] and Ulf Leonhardt[4]*

Transformation optics[1–6] is a concept used in some metamaterials[7–11] to guide light on a predetermined path. In this approach, the materials implement coordinate transformations on electromagnetic waves to create the illusion that the waves are propagating through a virtual space. Transforming space by appropriately designed materials makes devices possible that have been deemed impossible. In particular, transformation optics has led to the demonstration of invisibility cloaking for microwaves[12,13], surface plasmons[14] and infrared light[15,16]. Here, on the basis of transformation optics, we implement a microwave device that would normally require a dielectric singularity, an infinity in the refractive index. To fabricate such a device, we transmute[17] a dielectric singularity in virtual space into a mere topological defect in a real metamaterial. In particular, we demonstrate an omnidirectional retroreflector[18,19], a device for faithfully reflecting images and for creating high visibility from all directions. Our method is robust, potentially broadband and could also be applied to visible light using similar techniques.

Dielectric singularities are points where the refractive index n reaches infinity or zero, where electromagnetic waves travel infinitely slow or infinitely fast. Such singularities cannot be made in practice for a broad spectral range, but one can transmute them into topological defects of anisotropic materials[17]. Here is a brief summary of the underlying theoretical results[17]: imagine an isotropic index profile with a singularity in virtual space. Suppose that around the singularity the index profile is spherically symmetric, described by the function $n(r')$ in spherical coordinates $\{r', \vartheta', \phi'\}$. We use primes to distinguish virtual space from real space. Then we represent the virtual coordinates in real space $\{r, \vartheta, \phi\}$ by $\vartheta' = \vartheta$, $\phi' = \phi$ and the continuous function $r'(r)$. We require that $r'(r)$ obeys

$$n(r')\frac{\mathrm{d}r'}{\mathrm{d}r} = n_0 \quad \text{or, equivalently,} \quad r = r(r') = \frac{1}{n_0}\int n(r')\,\mathrm{d}r' \qquad (1)$$

where n_0 is a constant chosen such that beyond some radius a the virtual and the real coordinates coincide, $r' = r$ for $r \geq a$. The radius a defines the boundary of the device. Theory[4,17] shows that both the coordinate transformation and the virtual index profile are implemented by a material with the dielectric tensors

$$\varepsilon^i_j = \mu^i_j = \mathrm{diag}\left(\frac{n^2 r'^2}{n_0 r^2}, n_0, n_0\right) \qquad (2)$$

in spherical coordinates $x^i = \{r, \vartheta, \phi\}$. The tensors of the electric permittivity[20] ε^i_j and the magnetic permeability[20] μ^i_j describe an impedance-matched[20], anisotropic dielectric[20] with varying radial component. Such media are said to be anisotropic, because they respond to different electromagnetic-field components differently, as described by the tensors (2), although the device they constitute is spherically symmetric. As real space and virtual space coincide for $r \geq a$, the device with the properties (2) has the same physical effect as the index profile n, but the dielectric tensors remain finite, as long as $n(r')$ does not diverge faster than r'^{-1}. The direction of dielectric anisotropy, however, is not defined at $r = 0$, the position of the virtual singularity: the singularity has been transformed into a topological defect.

Consider, for example, the Eaton lens[18,19] illustrated in Fig. 1. The Eaton lens would reflect light back to where it came from, while faithfully preserving any image the light carries (apart from inverting the image). The lens is spherically symmetric, and so it would retroreflect light regardless of direction: it would make a perfect omnidirectional retroreflector. In contrast, conventional optical retroreflectors—'cat's eyes'—are made of mirrors and have a finite acceptance angle. A metallic sphere is an omnidirectional retroreflector as well, but only for rays that directly hit its centre. The sphere scatters off-centre light and distorts images, and so does a metallic rod in planar illumination. The Eaton lens is characterized by the index profile[18]

$$n = \sqrt{\frac{2a}{r'} - 1} \quad \text{for } r' < a \quad \text{and} \quad n = 1 \quad \text{for } r' \geq a \qquad (3)$$

To understand why the profile (3) acts as a perfect retroreflector, one can use the following analogy[21]: a light ray corresponds to the trajectory of a fictitious Newtonian particle that moves with energy E in the potential U, where $U - E = -n^2/2$ (in dimensionless units). The Eaton lens corresponds to the Kepler potential[21] $U = -a/r'$ for $r' < a$ and $U = -1$ outside the device, with total energy $E = -1/2$. The fictitious particle draws a half Kepler ellipse around the centre of attraction. So it leaves in precisely the opposite direction it came from[19]: light is retroreflected.

One sees that the profile (3) diverges with the power $-1/2$ and therefore an Eaton lens has never been made. However, we can transmute the singular isotropic profile into the regular but anisotropic material with the properties (2) by the coordinate transformation

$$r = \frac{2a}{n_0}\left[\arcsin\sqrt{\frac{r'}{2a}} + \sqrt{\frac{r'}{2a}\left(1 - \frac{r'}{2a}\right)}\right], \quad n_0 = 1 + \frac{\pi}{2} \qquad (4)$$

for $r' < a$ and $r = r'$ for $r' > a$, because this $r(r')$ solves the

[1]Temasek Laboratories, National University of Singapore, Singapore 119260, Singapore, [2]Centre for Superconducting and Magnetic Materials, Department of Physics, National University of Singapore, Singapore 117542, Singapore, [3]Institute of Theoretical Physics and Astrophysics, Masaryk University, Kotlarska 2, 61137 Brno, Czech Republic, [4]School of Physics and Astronomy, University of St Andrews, North Haugh, St Andrews, KY16 9SS, UK. *e-mail: ulf@st-andrews.ac.uk.

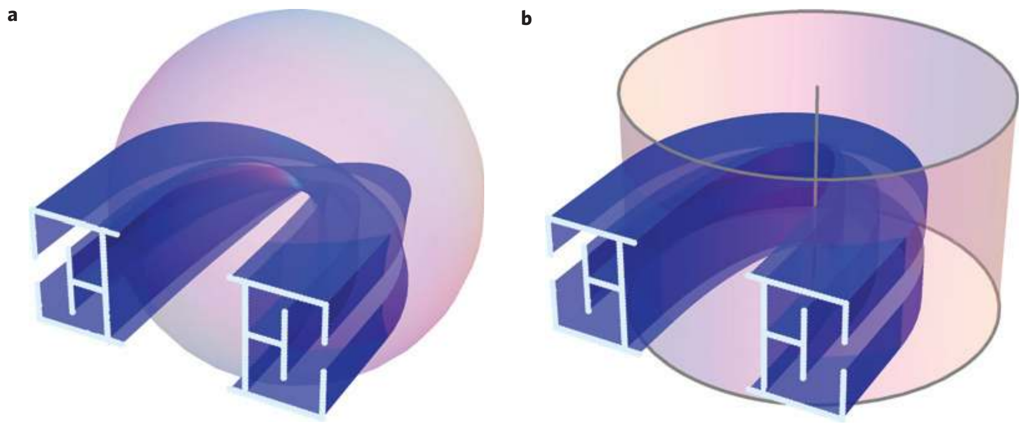

Figure 1 | Eaton lenses. a, Spherical lens. **b**, Cylindrical lens. An artist's impression of the retroreflection of light that carries an image, the letter 'E' for 'Eaton'. In the outgoing light, the image is inverted, but preserved (in **a**: flipped and upside down, in **b**: flipped). The implementation of an Eaton lens would require a singularity in the refractive index profile where the index tends to infinity, unless the singularity is transmuted into a harmless topological defect, as we demonstrate in this letter for the cylindrical lens with metamaterials for microwaves.

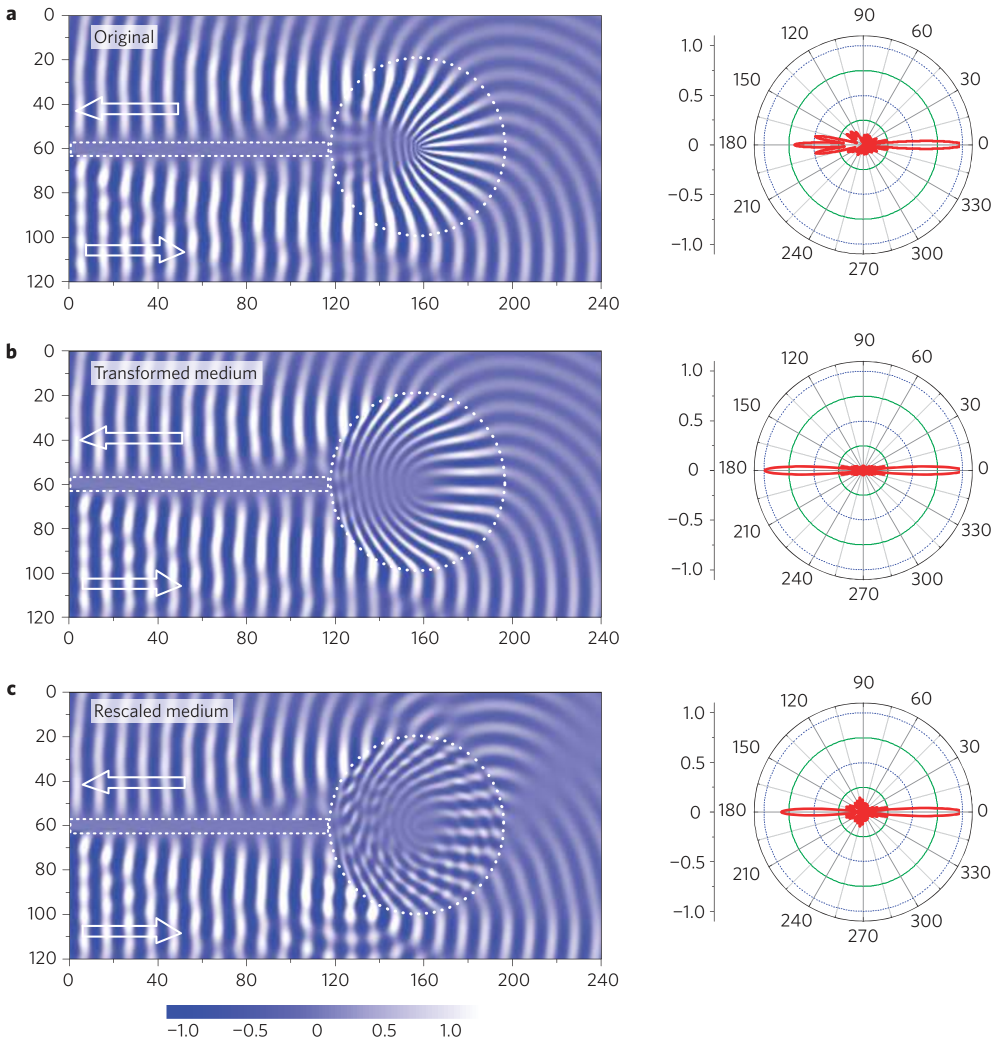

Figure 2 | Simulation of Eaton lenses. a–c, The left pictures show the distribution of the electric field at the original (**a**) and transformed Eaton lenses (**b**,**c**), with dielectric functions (5) and (6), respectively; the right pictures show the corresponding biscattering diagrams. The dotted circles in the left pictures mark the boundary of the device at radius a (40 mm); the dotted lines refer to an absorbing sheet that separates the incident and reflected electromagnetic waves, with their direction indicated by the arrows. The wavelength is $a/4$ and the scale is in millimetres for both axes. The biscattering diagrams refer to the electric field infinitely far away from the device. They show the ratio of the magnitude of the electric field as a function of angle, normalized by the largest value.

Figure 3 | The device. The split-ring resonators constitute a metamaterial for microwave radiation with the designed radial magnetic permeability (6). The rings were then filled with a white dielectric powder that generates the required electric permittivity of n_0^2 (not shown here).

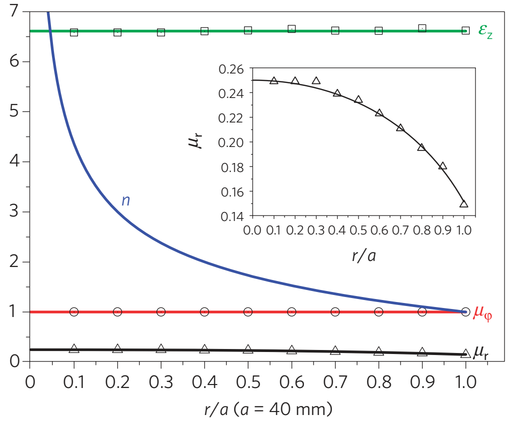

Figure 4 | Effective electromagnetic properties. The blue curve shows the index profile (3) of the original Eaton lens as a function of the radius r; the other curves show the rescaled dielectric functions (6) of the transmuted Eaton lens. The inset shows μ_r with magnified scale. The symbols are the dielectric functions calculated for the corresponding layers of the metamaterial.

integral (1) and approaches r' at $r' = a$. The singularity of the Eaton lens has been transformed away.

We found that this transmutation of singularities is remarkably robust: Fig. 2a,b compares numerical simulations of electromagnetic wave propagation in an ideal and a transmuted cylindrical Eaton lens. The cylindrical lens of Fig. 1b is characterized by its diagonal dielectric tensors in cylindrical coordinates $x^i = \{r, \varphi, z\}$, but we use the same functions (2)–(4) for the diagonal components ε_i and μ_i as in the case of the spherical lens,

$$\varepsilon_z = \mu_\varphi = n_0, \quad \mu_r = \frac{n^2 r'^2}{n_0 r^2} \tag{5}$$

We study the propagation of polarized electromagnetic waves in the $\{r, \varphi\}$ plane with the electric field pointing in the z direction. Such waves are not influenced by the other non-zero tensor components ε_r, ε_φ and μ_z. As Fig. 2a,b shows, the wave propagations in the two devices are nearly identical, although the theory (2)–(4) presumes a spherical transformation, not a cylindrical one. Moreover, the corresponding biscattering diagrams indicate that the transformed medium seems to be a better retroreflector than the numerically simulated Eaton lens, because of numerical problems associated with the singularity in the Eaton profile (3). Furthermore, Fig. 2c shows the effect of another modification of the ideal case (2)–(4) that is useful in practice: in this simulation, we rescale the dielectric functions in the device, but not in the air around it. Maxwell's equations are not changed if one rescales the dielectric functions (5) by the constant n_0 as

$$\varepsilon_z = n_0^2, \quad \mu_\varphi = 1, \quad \mu_r = \frac{n^2 r'^2}{n_0^2 r^2} \tag{6}$$

Consequently, the wave propagation in such media is the same as in materials with the dielectric functions (5). However, in reality the rescaling can be done only in the device, but not in air where $\varepsilon = \mu = 1$. So the impedance[20] is mismatched at the interface, which causes reflections[20]—scattering—but, as Fig. 2c shows, the phase profile of the outgoing wave is preserved, although the intensity is reduced. The associated biscattering diagram clearly indicates the loss in intensity, but not in directionality. As any incident wave can be represented as a superposition of plane waves, images will be faithfully reflected. The rescaled medium maintains the principal functionality of the Eaton lens.

Figure 3 shows our device. We built the transmuted Eaton lens from 10 concentric rings of low-loss printed circuit board (Rodgers RT6006 with 17.5 μmcopper coated on one side of 0.127 mm dielectric substrate with $\varepsilon = 6.2 - i0.01$). The rings have a height of 10 mm and are spaced with 4 mm distance until the radius of the outer ring reaches 40 mm. The rings carry three rows of split-ring resonators etched out from the copper of the circuit board (lengths 3.14 mm and heights 3.33 mm). The split-ring resonators create the required profile (6) of the radial magnetic permeability μ_r for microwave radiation at 8.9 GHz frequency (34 mm wavelength). They constitute a metamaterial[7–11], a material with dielectric properties created by subwavelength structures—the split-ring resonators in our case. The circuit-board rings were glued on a 0.1-mm-thick aluminium sheet that was prepatterned with concentric circular prints exactly fitting the rings. Then the rings were filled with dielectric powder (Emerson & Cuming Microwave Products) to generate the required electric permittivity (6) of n_0^2.

Figure 4 shows the curves of the dielectric functions. We designed the split-ring resonators by reverse-engineering where we calculate their dielectric response and modify their parameters until the calculated μ_r matches the required profile (6). However, each split-ring resonator interacts with its neighbours and cannot be considered on its own. For each individual resonator, we calculated the effective dielectric properties using Ansoft HFSS, assuming the resonator to constitute the elementary cell of an infinite lattice[22] (lattice constants 3.14, 4.00 and 3.33 mm in accordance with the dimensions of the resonators and the spacing of the circuit-board rings). In this way, we embed, in the modelling, the split-ring resonator into a lattice of its own kind. This procedure presumes that the dielectric properties do not vary much and it also ignores the curvature of the circuit-board rings, even at the inner ring of the device where the profile (6) contains a topological defect. Nevertheless, our experimental data prove that such a crudely transmuted Eaton lens works remarkably well in practice.

Figure 5 shows the results of our measurements. Our microwave source is a vector network analyser (HP8722D, Agilent Technologies) that we also use for detection. It has two ports connected by two coaxial cables (Megaphase 1GVT4), the feeding and the detecting port. To confine and scan the microwave radiation, we apply the parallel-plate electromagnetic field mapping system described elsewhere[23]. The microwave radiation is confined in the horizontal direction by two large aluminium boards at 11 mm spacing. The field is scanned by a sub-wavelength monopole probe antenna, a thin coaxial cable, inserted through a hole at the centre of the top plate. The bottom plate, carrying the device, is mounted on a computer-controlled stage that can move in two dimensions. The total scanning area covers $120 \times 240\,\text{mm}^2$ with a step resolution of 1 mm. On the bottom plate, pieces of 10-mm-thick microwave-absorbing foam were placed to define the incidence channel and suppress scattering at the boundaries. An absorbing

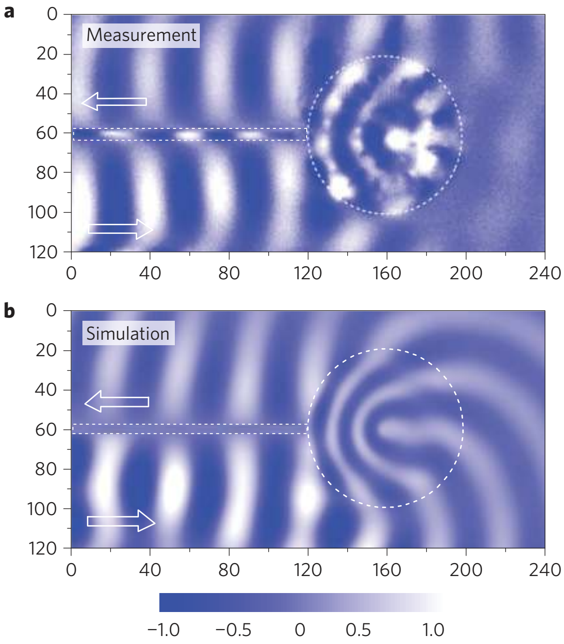

Figure 5 | Results. a,**b**, Measurement results (**a**) compared with simulation (**b**). Description as for the left pictures of Fig. 2, except that here the wavelength is 34 mm (0.85*a*).

sheet segregates the incidence channel from the reflected radiation. The sheet was made of a 0.1-mm-thick copper tape sandwiched between two 1.5-mm-thick layers of magnetically loaded silicone absorber (ECCOSORB).

As Fig. 5a shows, the measured field inside the device is perturbed by the graininess of the metamaterial and its ring structure, but the outgoing wave is in very good agreement with the numerical simulation for a smooth dielectric profile shown in Fig. 5b. In simulations, we even reduced the number of rings to 5, and still observed a good performance of the transmuted Eaton lens. There we approximated the device by five equidistant uniform layers with constant dielectric properties (6). Our crudely approximated prototype preserves the functionality of the ideal Eaton lens, which indicates that the transmutation of singularities[17] can be remarkably robust and reliable in practice. As the required dielectric properties (2) lie within a finite range, such devices can, in principle, work over a broad range of the spectrum and similar devices[15,16,24–28] could even operate in the visible.

Received 17 March 2009; accepted 27 May 2009; published online 28 June 2009

References

1. Dolin, L. S. On the possibility of comparing three-dimensional electromagnetic systems with non-uniform anisotropic fillings. *Isv. Vusov* **4**, 964–967 (1961).
2. Leonhardt, U. Optical conformal mapping. *Science* **312**, 1777–1780 (2006).
3. Pendry, J. B., Schurig, D. & Smith, D. R. Controlling electromagnetic fields. *Science* **312**, 1780–1782 (2006).
4. Leonhardt, U. & Philbin, T. G. General relativity in electrical engineering. *New J. Phys.* **8**, 247 (2006).
5. Shalaev, V. M. Transforming light. *Science* **322**, 384–386 (2008).
6. Leonhardt, U. & Philbin, T. G. Transformation optics and the geometry of light. Preprint at <http://arxiv.org/abs/0805.4778> (2008).
7. Milton, G. W. *The Theory of Composites* (Cambridge Univ. Press, 2002).
8. Smith, D. R., Pendry, J. B. & Wiltshire, M. C. K. Metamaterials and negative refractive index. *Science* **305**, 788–792 (2004).
9. Soukoulis, C. M., Linden, S. & Wegener, M. Negative refractive index at optical wavelengths. *Science* **315**, 47–49 (2007).
10. Sarychev, A. K. & Shalaev, V. M. *Electrodynamics of Metamaterials* (World Scientific, 2007).
11. Zhang, X. & Liu, Z. W. Superlenses to overcome the diffraction limit. *Nature Mater.* **7**, 435–441 (2008).
12. Schurig, D. *et al.* Metamaterial electromagnetic cloak at microwave frequencies. *Science* **314**, 977–980 (2006).
13. Liu, R. *et al.* Broadband ground-plane cloak. *Science* **323**, 366–369 (2009).
14. Smolyaninov, I. I., Hung, Y. J. & Davis, C. C. Two-dimensional metamaterial structure exhibiting reduced visibility at 500 nm. *Opt. Lett.* **33**, 1342–1344 (2008).
15. Valentine, J., Li, J., Zentgraf, T., Bartal, G. & Zhang, X. An optical cloak made of dielectrics. *Nature Mater.* **8**, 568–571 (2009).
16. Gabrielli, L. H., Cardenas, J., Poitras, C. B. & Lipson, M. Cloaking at optical frequencies. *Nature Photon.* doi: 10.1038/nphoton.2009.117 (2009); preprint at <http://arxiv.org/abs/0904.3508> (2009).
17. Tyc, T. & Leonhardt, U. Transmutation of singularities in optical instruments. *New J. Phys.* **10**, 115038 (2008).
18. Eaton, J. E. *An Extension of the Luneburg–Type Lenses* (Rep. No. 4110, Naval Res. Lab., 1953).
19. Hannay, J. H. & Haeusser, T. M. Retroreflection by refraction. *J. Mod. Opt.* **40**, 1437–1442 (1993).
20. Jackson, J. D. *Classical Electrodynamics* (Wiley, 1999).
21. Leonhardt, U. Notes on conformal invisibility devices. *New J. Phys.* **8**, 118 (2006).
22. Smith, D. R. & Pendry, J. B. Homogenization of metamaterials by field averaging. *J. Opt. Soc. Am. B* **23**, 391–403 (2006).
23. Zhao, L., Chen, X. & Ong, C. K. Visual observation and quantitative measurement of the microwave absorbing effect at X band. *Rev. Sci. Instrum.* **79**, 124701 (2008).
24. Cai, W. S., Chettiar, U. K., Kildishev, A. V. & Shalaev, V. M. Optical cloaking with metamaterials. *Nature Photon.* **1**, 224–227 (2007).
25. Liu, N. *et al.* Three-dimensional photonic metamaterials at optical frequencies. *Nature Mater.* **7**, 31–37 (2008).
26. Rill, M. S. *et al.* Photonic metamaterials by direct laser writing and silver chemical vapour deposition. *Nature Mater.* **7**, 543–546 (2008).
27. Valentine, J. *et al.* Three-dimensional optical metamaterial with a negative refractive index. *Nature* **455**, 376–379 (2008).
28. Yao, J. *et al.* Optical negative refraction in bulk metamaterials of nanowires. *Science* **321**, 930–930 (2008).

Acknowledgements

Y.G.M. and C.K.O. are supported by the Defense Science and Technology Agency under the Defense Innovative Research Program, Singapore (DSTA-NUS-DIRP/2004/02), T.T. acknowledges the grants MSM0021622409 and MSM0021622419 and U.L. is supported by a Royal Society Wolfson Research Merit Award.

Author contributions

Y.G.M. and C.K.O. made contributions to the numerical simulations, device design, implementation and the experiment, T.T. and U.L. made contributions to the theory and U.L. suggested this project and wrote the paper.

Additional information

Reprints and permissions information is available online at http://npg.nature.com/reprintsandpermissions. Correspondence and requests for materials should be addressed to U.L.